

# Mycobactin-mediated iron acquisition within macrophages

Minkui Luo, Evgeny A Fadeev & John T Groves

**Restricting the availability of iron is an important strategy for defense against bacterial infection<sup>1–3</sup>. *Mycobacterium tuberculosis* survives within the phagosomes of macrophages; consequently, iron acquisition is particularly difficult for *M. tuberculosis*, because the phagosomal membrane is an additional barrier for its iron access<sup>4,5</sup>. However, little is known about the iron transport and acquisition pathways adapted by this microbe *in vivo*<sup>6</sup>. Extracellular iron sources are usually mobilized by hydrophilic siderophores<sup>7,8</sup>. Here, we describe direct evidence that mycobactins, the lipophilic siderophores of mycobacteria, efficiently extract intracellular macrophage iron. The metal-free siderophore is diffusely associated with the macrophage membrane, ready for iron chelation. Notably, the mycobactin-metal complex accumulates with high selectivity in macrophage lipid droplets, intracellular domains for lipid storage and sorting<sup>9,10</sup>. In our experiments, these mycobactin-targeted lipid droplets were found in direct contact with phagosomes, poised for iron delivery. The existence of this previously undescribed iron acquisition pathway indicates that mycobacteria have taken advantage of endogenous macrophage mechanisms for iron mobilization and lipid sorting for iron acquisition during infection. The pathway could represent a new target for the control of mycobacterial infection.**

Macrophages stand as gatekeepers for the host immune defense against invading bacteria by using an array of antimicrobial devices<sup>11</sup>. Among the various compensations are the depletion of iron in serum transferrin<sup>11,12</sup> and the increased synthesis of ferritins<sup>13,14</sup>. Although macrophage cells can internalize a variety of intruding microbes through phagocytosis and degrade them within phagolysosomes, pathogenic mycobacteria have developed creative means to avoid the fatal fusion with lysosomes and thus multiply within these host cells<sup>4,5</sup>. *M. tuberculosis*, one of the most insidious macrophage-targeted strains, currently infects one-third of the world's population, and there are increasing reports of multidrug-resistant strains (<http://www.who.int/mediacentre/factsheets>). Here, we report a rapid, mycobactin-mediated iron acquisition process and subsequent mycobactin-specific iron transport within macrophages that exploits the ready membrane permeability, dynamic diffusibility and high iron affinity of these small lipophilic siderophores. This iron acquisition process is stimulated by

ferric transferrin or cobalt(III) transferrin, implicating the iron transport apparatus, rather than the iron in transferrin, as the primary target. Our findings regarding mycobactin-mediated iron acquisition suggest new targets for combating mycobacterial infections<sup>15</sup>.

We examined the interactions of mycobactin J, a siderophore from *Mycobacterium paratuberculosis* (MJ, **1**, **Fig. 1a**), with human macrophage cells in culture by monitoring the appearance of MJ-iron complex (Fe-MJ, **2**). Approximately 20% of the added MJ was recovered as Fe-MJ under these conditions, in contrast to less than 5% conversion in the absence of macrophages (**Fig. 1b**). This result indicates that extracellularly added MJ translocated through the plasma membrane and acquired intracellular iron from macrophages. Similar conversion to Fe-MJ was observed in the presence of a 30-fold excess of the water-soluble iron(III) chelator desferrioxamine, confirming that this MJ-mediated iron chelation is an intracellular process.

The iron-transport protein transferrin is known to promote the growth of mycobacteria<sup>16</sup>. We found that added human transferrin (hTf) stimulated MJ-mediated iron acquisition from macrophages at low, physiologically significant levels (10  $\mu$ M hTf)<sup>17</sup>. The conversion of MJ to Fe-MJ nearly doubled in the presence of hTf (**Fig. 1b**). This hTf-triggered conversion was significantly suppressed at low temperatures (gray columns in **Fig. 1c**), reaching a level at 4 °C similar to that observed in the absence of hTf (compare **Fig. 1b,c**).

Notably, cobalt(III) transferrin (Co-Tf) was a more effective agonist than hTf for triggering iron release from macrophages to MJ (**Fig. 1d**). This result suggests that initiating transferrin receptors also mobilized internal iron stores for this MJ-mediated iron acquisition. By contrast, the more labile Ga(III) and Al(III) transferrin complexes not only did not stimulate iron release from macrophages to MJ, but also greatly suppressed the basal recovery of Fe-MJ (**Fig. 1d**).

We examined the distribution of MJ and Fe-MJ between aqueous phase and macrophages by incubating MJ or Fe-MJ in 10<sup>5</sup> cells per ml macrophage culture for 0.5 h. Notably, we found that 70–90% of the added MJ or Fe-MJ was recovered from the aqueous phase under these conditions. We then recovered both aqueous-phase Fe-MJ and total Fe-MJ after the 24-h incubation of MJ in macrophage culture, in either the presence or the absence of hTf. Here, Fe-MJ from the aqueous phase also accounted for 80% of the total recovered Fe-MJ (**Fig. 2a**). These observations are consistent with the cell–aqueous phase partition coefficients for MJ (**Fig. 2b**) and Fe-MJ (**Fig. 2c**) of  $2.4 \times 10^{-6}$  ml per cell and  $9.8 \times 10^{-7}$  ml per cell, respectively. The

Department of Chemistry, Princeton University, Princeton, New Jersey 08544, USA. Correspondence should be addressed to J.T.G. ([jtgroves@princeton.edu](mailto:jtgroves@princeton.edu)).

Published online 3 July 2005; doi:10.1038/nchembio717

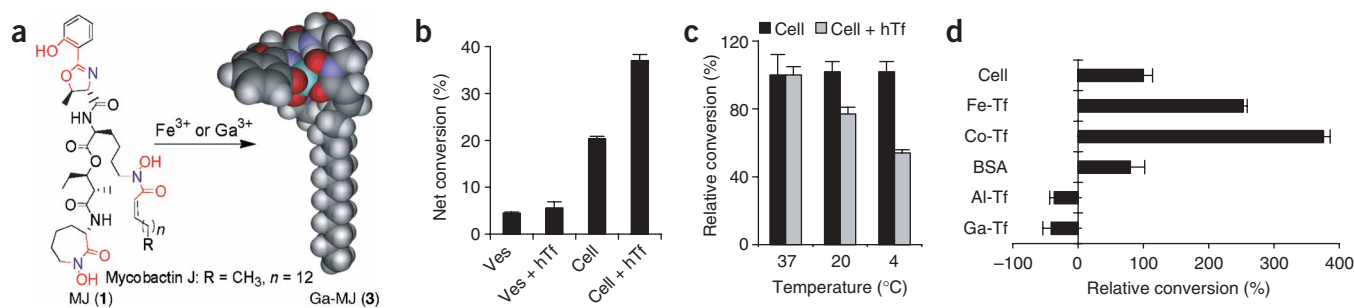


**Figure 1** MJ-mediated iron acquisition. (a) The structure of MJ and Ga-MJ. The chelating moieties of MJ are highlighted in red (oxygen) and blue (nitrogen). A representative three-dimensional structure of Ga-MJ; C, dark gray; H, light gray; O, red; N, blue; Ga, cyan. (b) The conversion to Fe-MJ. MJ targets macrophage intracellular iron, a process promoted by hTf. Ves, 0.05 mM vesicle; Ves + hTf, 0.05 mM vesicle with 10  $\mu$ M hTf; Cell, macrophages; Cell + hTf, macrophages supplied with 10  $\mu$ M hTf. Net conversion (%) is the ratio of the actual conversion to Fe-MJ to the theoretical 100% conversion. (c) The effect of temperature on MJ-mediated iron acquisition. Iron transfer from macrophages to MJ was insensitive to temperature, but hTf-triggered iron transfer was inhibited at low temperatures. Relative conversion of 100% was defined as the conversion to Fe-MJ at 37  $^{\circ}$ C, in either the presence (gray column) or the absence (black column) of 10  $\mu$ M hTf. (d) Co(III)-Tf-stimulated iron acquisition of MJ. All the experiments were carried out as described in **Figure 1b** in either the absence ("Cell") or the presence of 10  $\mu$ M hTf ("hTf"), Co(III)-Tf ("Co-Tf"), Al(III)-Tf ("Al-Tf"), Ga(III)-Tf ("Ga-Tf") or 1 mg ml<sup>-1</sup> bovine serum albumin as the control ("BSA"). Relative conversion of 100% was defined as the conversion at 37  $^{\circ}$ C without hTf. Negative relative conversion values correspond to the less-than-basal recovery of Fe-MJ. Plots show means of triplicates with s.e.m.

moderate membrane affinity of Fe-MJ is also consistent with its lipid-aqueous phase partition coefficient ( $K_x = 3 \times 10^5$ ) that was obtained with lipid vesicles as a model membrane (unpublished result). These results indicate that MJ and its iron complex can freely diffuse among infected macrophages, mycobacteria and the medium, a feature that would facilitate access to the host iron pool and the transport of iron to the bacterial pathogens.

To further examine the dynamic redistribution of added Fe-MJ and MJ within cells, we used fluorescent confocal microscopy to visualize MJ and gallium-MJ complex (Ga-MJ, **3**, **Fig. 1a**) as an Fe-MJ surrogate. Lipid-phase Ga-MJ displays a pronounced fluorescence emission that was very useful for these experiments. Upon incubation in macrophage culture for 20–120 min, Ga-MJ was found preferentially localized in a single intracellular structure (**Fig. 3a**). This special locus was determined to be the lipid droplet by the observed colocalization of Ga-MJ and Nile red in these regions (**Fig. 3b**). Lipid droplets are important intracellular domains for lipid storage

and sorting and for the synthesis of host immune-defense mediator eicosanoids<sup>9,10</sup>. MJ, by contrast, was homogeneously distributed among lipid regions of macrophages (**Fig. 3c**), similar to other hydrophobic fluorescent markers such as LysoTracker (a lysosome marker from Invitrogen) and FM 4-64 (an endo- and exocytosis marker from Molecular Probes). Consequently, this unusual affinity of Ga-MJ for lipid droplets must be attributed to a specific interaction rather than general hydrophobic effects. Fe-MJ should share this lipid-droplet affinity, because gallium siderophores are good structural analogs of the corresponding ferric complexes on the basis of their similar ionic radius, charge and metal-coordinating properties<sup>18</sup>.

We further noticed that Ga-MJ-laden lipid droplets displayed direct contacts with phagosomes containing fluorescent *Escherichia coli* (**Fig. 3d**). This finding suggests that mycobacteria have exploited host lipid trafficking for mycobactin-mediated iron delivery by recruiting Fe-MJ to lipid droplets within macrophages. The subsequent migration of Fe-MJ-laden lipid droplets to phagosomes would thus facilitate iron delivery to phagosomal mycobacteria. During bacterial infection and after phagocytosis, lipid droplets in human lung macrophages are reported to move to phagosomes and discharge their contents there<sup>19,20</sup>. Ironically, this lipid-droplet trafficking by the host immune defense seems to be the vector for iron delivery to macrophage-niche mycobacteria.

Three lines of evidence presented here show that MJ and Fe-MJ rapidly translocate through cell membranes and maintain a dynamic

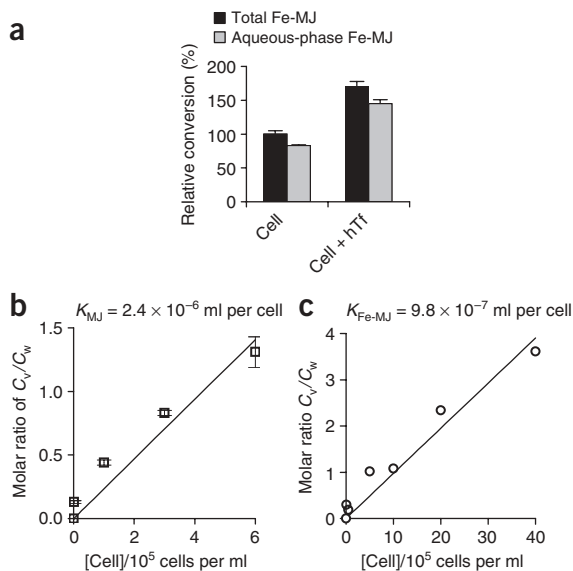


**Figure 2** Membrane partitioning of MJ and Fe-MJ. (a) The cell–aqueous phase distribution of Fe-MJ upon iron release to MJ. Both aqueous-phase Fe-MJ (gray) and total Fe-MJ (black) were recovered after the 24-h incubation of MJ in macrophage culture (1  $\times 10^5$  cells per ml), in either the presence ("Cell + hTf") or the absence ("Cell") of hTf. Here, Fe-MJ from the aqueous phase accounted for 80% of the total recovered Fe-MJ. The total conversion in the absence of hTf was set as 100% relative conversion. (b,c) Measurements of cell–aqueous phase partition coefficients of MJ and Fe-MJ, respectively.  $C_v$  and  $C_w$  stand for lipid-phase and aqueous-phase amounts of MJ or Fe-MJ, respectively. Partition coefficients of MJ and Fe-MJ were obtained with  $K_{MJ} = 2.4 \times 10^{-6}$  ml per cell and  $K_{Fe-MJ} = 9.8 \times 10^{-7}$  ml per cell ( $C_v/C_w = K \times [Cell]$ ). Panels **a** and **b** show means of triplicates with s.e.m.

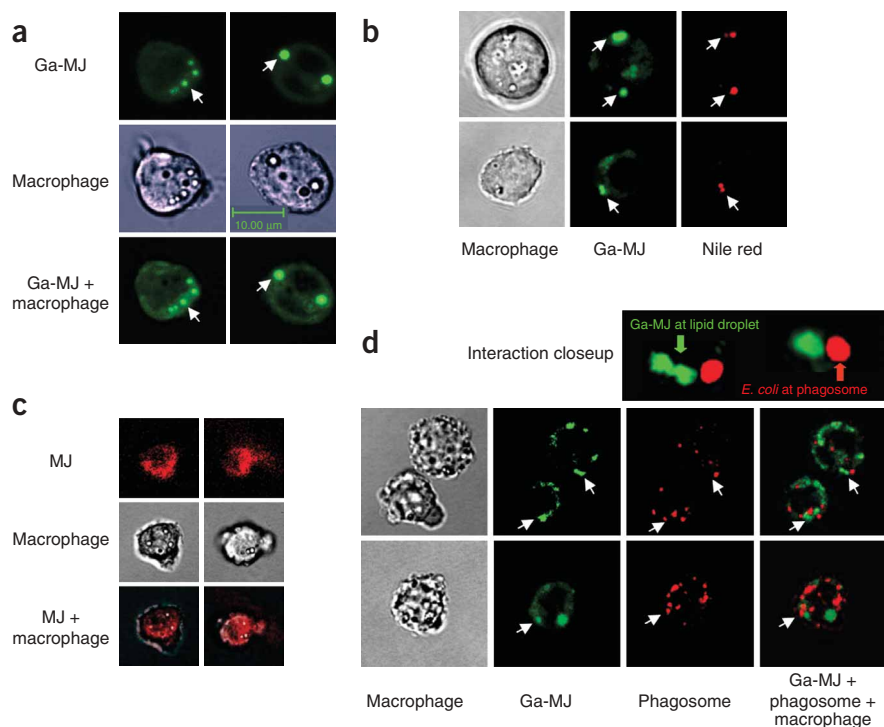


**Figure 3** Distribution patterns of MJ and Ga-MJ within macrophages. **(a)** Fluorescent confocal images of the intracellular distribution of Ga-MJ in macrophages. Ga-MJ has a preferential affinity for lipid droplets, as shown by the arrows. Images from top to bottom: Ga-MJ (green channel), transmission images of macrophages and the overlap of both. **(b)** Identifying the preferential locus as lipid droplets for Ga-MJ diffusion. The Nile red-stained lipid droplets (red channel) were colocalized with the Ga-MJ-preferred locus (green channel). Images from left to right: transmission images of macrophages, Ga-MJ (green channel) and Nile red (red channel). **(c)** Fluorescent confocal images of the intracellular distribution of MJ in macrophages. MJ loses the lipid droplet-affinity pattern in contrast to Fe-MJ. Images from top to bottom: MJ (red channel), transmission images of macrophages and the overlap of both. **(d)** Co-staining of Ga-MJ and fluorescence-labeled *E. coli* phagosomes. Arrows show the contacting regions for Ga-MJ-stained lipid droplets (green channel) and fluorescence-labeled *E. coli* phagosomes (red channel). Left to right: transmission images of macrophages, Ga-MJ (green channel), phagosomes (red channel) and the overlap of all three. The upper right profiles are two representative images of the interaction between Ga-MJ-laden lipid droplets and *E. coli*-residing phagosomes.

distribution between the medium and cellular lipid components. (i) Extracellularly added MJ acquires intracellular iron from macrophages, and a large portion of Fe-MJ was recovered from the aqueous phase (Figs. 1b and 2b). (ii) Both MJ and Fe-MJ showed only moderate cell-aqueous phase partition coefficients (Fig. 2b,c). (iii) Upon the incubation of extracellular MJ and Ga-MJ with macrophages, the diffusion of the two amphiphiles reached equilibrium within 20 min, with Ga-MJ being rapidly translocated to intracellular lipid droplets (Fig. 3a,b). Lipophilic mycobactins have been recovered from both *M. tuberculosis* cells and growth media<sup>21</sup>, consistent with mycobactin diffusion. Similar diffusive properties have been reported for a variety of amphiphilic siderophores<sup>22,23</sup>. Mycobactin derivatives have also been shown recently to be antigens for activated T cells<sup>24</sup>.

Macrophages are responsible for clearing senescent red blood cells and thus are often richly loaded with iron<sup>25</sup>. Macrophage iron loading is even more serious during infection, because approximately 30% of the circulating iron is withdrawn from serum to macrophages under such conditions<sup>11,12</sup>. As we have shown that extracellularly added MJ can chelate macrophage intracellular iron (Fig. 1), it seems that this intracellular iron(III) pool is accessed by lipophilic

mycobactins, because of their ready diffusibility and membrane permeability. The iron source could be ferritin or intracellular organelle-bound iron<sup>26</sup>.

In the presence of hTf or Co-Tf, MJ-mediated iron acquisition from macrophages was further stimulated (Fig. 1). This increased iron release to MJ must be a metabolically accelerated process, because it was completely suppressed at lower temperatures. In the presence of hTf, two components contributed to the total iron release to MJ: hTf-independent iron acquisition from the macrophage intracellular iron pool and the hTf-stimulated iron release. For the latter, we ruled out the possibility that lipophilic MJ directly mobilized iron from hTf, because the iron transfer from hTf to mycobactin *in vitro* is a slow process (Fig. 1b). Furthermore, Co-Tf was an even better agonist than hTf for this stimulation process. We argue that MJ mobilizes iron from pre-existing intracellular sources and that this process is further promoted by hTf, presumably involving hTf-receptor interactions.

On the basis of these data, we propose a new iron-acquisition mechanism for macrophage-niche mycobacteria (Fig. 4). Upon taking residence in early phagosomes through macrophage-mediated phagocytosis, pathogenic mycobacteria assemble mycobactins and the corresponding transport systems through *mbtA-J* gene products<sup>27</sup>. The newly synthesized mycobactins then diffuse into the host macrophage (Fig. 4, step 1). Because of the moderate membrane affinity and ready membrane permeability of mycobactins, a dynamic distribution of mycobactins is rapidly built up between the medium and cellular lipid components. Subsequently, mycobactins mobilize iron from the macrophage intracellular iron pool (step 2). Mycobactins may also acquire iron from endocytosis-internalized transferrin<sup>16</sup>. It is likely that this pathway becomes dominant for those macrophage cells that have intrinsically low iron storage but are rapidly mobilizing iron from transferrin. Upon chelating iron, mycobactins are converted into ferric mycobactins that also rapidly diffuse through the cellular milieu and reach a dynamic distribution between the medium and cellular lipid components (step 3). Ferric mycobactin is further recruited to lipid droplets delivered through lipid trafficking to the phagosomes (step 4). These properties would provide macrophage-ensconced mycobacteria with the mycobactin-mobilized iron. All these observations suggest that the dynamics of iron mobilization, membrane trafficking and lipid sorting within macrophages have been exploited to deliver iron to mycobacteria residing in phagosomes.

This model accommodates previous studies of pathogenic mycobacteria and their siderophore products. First, an *M. tuberculosis* mutant incapable of producing mycobactins shows restricted growth both within macrophages and under iron limitation<sup>21</sup>. Therefore, mycobactins must be virulence factors during infection. Second, the administration of mycobactins and ferritins together, but not of either

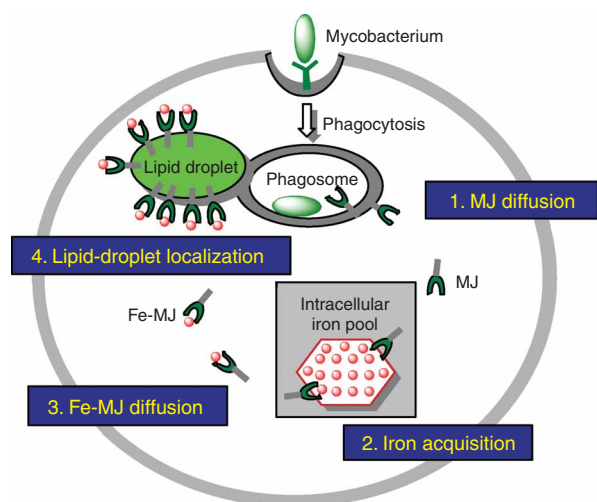


**Figure 4** Our proposed MJ-mediated iron-acquisition pathway for macrophage-niche mycobacteria. Mycobacteria are initially internalized through phagocytosis and reside in phagosomes. The newly assembled mycobactins diffuse away from mycobacteria and rapidly distribute between bulk medium and cellular lipid components (1. MJ diffusion). These diffusible mycobactins access intracellular iron pool and mobilize iron there (2. Iron acquisition). This process is also stimulated by hTf and Co(III)-Tf. Ferric mycobactins then diffuse away from the intracellular iron pool (3. Fe-MJ diffusion). Finally, ferric mycobactins preferentially localize to lipid droplets, where they are ready to be delivered to lipid droplet-attached phagosomes residing in mycobacteria (4. Lipid-droplet localization).

one alone, promotes the fast growth of *M. tuberculosis in vitro*<sup>28</sup>. Both of these results are consistent with MJ-mediated iron acquisition from the macrophage intracellular iron pool (Fig. 4).

Lipophilic mycobactins have been considered as intra-envelope, short-term iron storage molecules by their interaction with hydrophilic carboxymycobactins, which are responsible for extracellular iron acquisition<sup>29</sup>. Our studies of MJ indicate that the amphiphile directly acquires macrophage intracellular iron through membrane diffusion. The behavior of MJ revealed here could have a broad impact on understanding and management of mycobacterial infection. In particular, the discovery that Ga-MJ and, presumably, Fe-MJ accumulate in lipid droplets, whereas MJ does not preferentially bind to that site, suggests that lipid droplets could be a key locus for iron restriction. Agents that target the Ga-MJ binding site could serve to inhibit iron transport to mycobacteria. Alternatively, antimicrobial agents could be designed that mimic the mycobactins and accumulate in the lipid droplets. Mycobactin-gallium complexes themselves could be potential antibiotics, because they could deliver gallium specifically to intracellular mycobacteria instead of to other host cells; it has been reported that gallium disrupts iron metabolism in mycobacteria<sup>30</sup>. In conclusion, we have described several new aspects of the molecular choreography of mycobactin-mediated iron acquisition within human macrophage cells. The lipid-droplet interaction in particular indicates a lively orchestration of these host-pathogen dynamics, which has implications for intervention and possible controls.

## METHODS

**Ga-MJ synthesis.** Ga-MJ was prepared as follows: 30 mg of MJ was dissolved in 0.7 ml of CD<sub>3</sub>OD in a 5-mm NMR tube and titrated with a saturated CD<sub>3</sub>OD solution of gallium acetylacetonate (Sigma) until the uncomplexed MJ <sup>1</sup>H-NMR signals completely disappeared and a new set of signals developed.

Acetylacetonate was removed upon subsequent evaporation under vacuum. The Ga-MJ sample was purified through a short column in the barrel of a 5-cc hypodermic syringe (bed height ~5 cm, diameter ~1 cm, 60 mesh silica) and eluted with 0–15% (v/v) methanol in chloroform to give pure Ga-MJ. The <sup>1</sup>H NMR spectrum of Ga-MJ is shown in the **Supplementary Methods** online. The chromatographic process could be easily monitored by ultraviolet (UV) irradiation at 365 nm, as Ga-MJ shows a bright blue fluorescence.

**HPLC analysis for Fe-MJ.** Varian ProStar & PrepStar HPLC and a Waters Delta Pak 5 μ C18-300Å column were used with 3:7 (v/v) H<sub>2</sub>O/CH<sub>3</sub>CN as the eluting solution under all conditions. The intensities of the peak with retention time 43 min at 460 nm were integrated and normalized to the amount of Fe-MJ. Macrophages (final concentration, 10<sup>5</sup> cells per ml) or 0.05 mM dimyristoyl phosphatidylcholine vesicles as controls were preincubated in RPMI 1640 medium at 37 °C for 4 h, after which MJ was added (final concentration, 1.5 μM). The media were incubated for 24 h under various conditions, such as in the presence or absence of Tf, at various temperatures or in the presence of different concentrations of desferrioxamine mesylate salt. Three 4-ml aliquots of the medium were collected and lysed using Dounce homogenizers. Lipophilic components were extracted into 3.5 ml of chloroform and the mixture was centrifuged at 2,000g for 8 min. The organic layer extraction of 2.5 ml was subjected to a stream of argon to vaporize chloroform. The dried mixture was dissolved into 400 μl of CH<sub>3</sub>CN, of which 200 μl of solution was injected into HPLC. The peak intensity of 100% conversion to Fe-MJ was obtained by the incubation of 1.5 μM Fe-MJ in the medium, after the aforementioned workup.

**Cell-aqueous phase distributions of MJ and Fe-MJ.** After the conversion from MJ to Fe-MJ, aqueous-phase Fe-MJ was obtained by the separation of the supernatant medium from macrophage cells by centrifugation at 400g for 5 min. The aliquot of recovered supernatant was subjected to chloroform extraction and HPLC analysis as described in the previous section. For measurements of the cell-aqueous phase partition coefficient of Fe-MJ, 1.0 μM Fe-MJ was incubated in RPMI 1640 medium at 37 °C for half an hour in the presence of various concentrations of macrophage cells. Then the supernatant was separated and analyzed as described in the previous section. For the partition coefficient of MJ, before the HPLC analysis, a ten-fold excess of iron citrate was added into an MJ-CH<sub>3</sub>CN solution, and the mixture was incubated for 2 h for complete conversion from MJ to Fe-MJ. The amounts of aqueous-phase and total MJ and Fe-MJ,  $C_w$  and  $C_{total}$ , respectively, were used to calculate  $C_v/C_w$  according to the relationship  $C_v/C_w = (C_{total} - C_w)/C_w$ . The partition coefficient,  $K$ , was defined according to the following equation:  $C_v/C_w = K \times [\text{Cell}]$ , in which  $[\text{Cell}]$  is the concentration of macrophage cells (cells per ml) and  $C_v$  is the amount of lipid-phase MJ or Fe-MJ.

**Fluorescent confocal microscopy.** Fluorescent confocal microscopy experiments were carried out with a Bio-Rad MRC 600 confocal microscope. Phenol red-free RPMI 1640 medium supplied with NaHCO<sub>3</sub> and HEPES buffer was used in all cases. Ga-MJ or MJ (2 μM) was incubated in macrophage culture with 10<sup>5</sup> cells per ml for 2 h. Fluorescent confocal images were taken *in situ* by 364-nm excitation of MJ and Ga-MJ. Lipid-phase MJ and Ga-MJ show excellent fluorescence emissions around 364 nm, whereas aqueous-phase MJ shows no significant fluorescence. Ga-MJ–Nile red (lipid-droplet marker) colocalization experiments were carried out similarly, except for the incubation of 2 μM Ga-MJ and 0.1 μg ml<sup>-1</sup> of Nile red together. An argon laser was used to excite Nile red at 488 nm. For co-staining of Ga-MJ and fluorescence-labeled *E. coli* phagosomes, fluorescence-labeled *E. coli* were incubated in macrophage culture with 5 × 10<sup>5</sup> cells per ml for 24 h, during which macrophages were centrifuged down and then resuspended twice to increase phagocytosis of *E. coli*. Finally, macrophages were separated from medium, suspended in *E. coli* and then diluted to 1 × 10<sup>5</sup> cells per ml. Ga-MJ (2 μM) was added and incubated for another 2 h. Fluorescent confocal images were taken *in situ* with the laser UV line at 364 nm to excite Ga-MJ and with the 488-nm line to visualize phagosomes labeled with fluorescent *E. coli*.

**Materials, cell cultures and NMR spectra.** See **Supplementary Methods** for details.

Note: Supplementary information is available on the Nature Chemical Biology website.

#### ACKNOWLEDGMENTS

The authors thank M. Marlow for providing facilities and technical assistance with cell cultures, J. Goodhouse for fluorescent confocal microscopy and F. Morel and B. Ward for iron-labeling experiments. Support of this work by the US National Science Foundation (CHE-0221978) through the Environmental Molecular Science Institute (CEBIC) at Princeton University is gratefully acknowledged.

#### COMPETING INTERESTS STATEMENT

The authors declare that they have no competing financial interests.

Received 21 April; accepted 13 June 2005

Published online at <http://www.nature.com/naturechemicalbiology/>

- Flo, T.H. *et al.* Lipocalin 2 mediates an innate immune response to bacterial infection by sequestering iron. *Nature* **432**, 917–921 (2004).
- Ferreras, J.A., Ryu, J.S., Lello, F.D., Tan, D.S. & Quadri, L.E.N. Small-molecule inhibition of siderophore biosynthesis in *Mycobacterium tuberculosis* and *Yersinia pestis*. *Nat. Chem. Bio.* **1**, 29–32 (2005).
- Fluckinger, M., Hass, H., Merschak, P., Glasgow, B.J. & Redl, B. Human tear lipocalin exhibits antimicrobial activity by scavenging microbial siderophores. *Antimicrob. Agents Chemother.* **48**, 3367–3372 (2004).
- Pieters, J. Entry and survival of pathogenic mycobacteria in macrophages. *Microbes Infect.* **3**, 249–255 (2001).
- Rhoades, E.R. & Ullrich, H.J. How to establish a lasting relationship with your host: lessons learned from *Mycobacterium spp.* *Immunol. Cell Biol.* **78**, 301–310 (2000).
- Schaible, U.E. & Kaufmann, S.H.E. Iron and microbial infection. *Nat. Rev. Microbiol.* **2**, 946–953 (2004).
- Albrecht-Gary, A.M. & Crumbliss, A.L. Coordination chemistry of siderophores: thermodynamics and kinetics of iron chelation and release. *Met. Ions Biol. Syst.* **35**, 239–327 (1998).
- Ratledge, C. & Dover, L.G. Iron metabolism in pathogenic bacteria. *Annu. Rev. Microbiol.* **54**, 881–941 (2000).
- Melo, R.C., D'Avila, H., Fabrino, D.L., Almeida, P.E. & Bozza, P.T. Macrophage lipid body induction by Chagas disease in vivo: putative intracellular domains for eicosanoid formation during infection. *Tissue Cell* **35**, 59–67 (2003).
- Yu, W. *et al.* Co-compartmentalization of MAP kinases and cytosolic phospholipase A(2) at cytoplasmic arachidonate-rich lipid bodies. *Am. J. Pathol.* **152**, 759–769 (1998).
- Burke, B. & Lewis, C.E. *The Macrophage* (Oxford University Press, Oxford, UK, 2002).
- Torti, S.V. *et al.* The molecular cloning and characterization of murine ferritin heavy chain, a tumor necrosis factor-inducible gene. *J. Biol. Chem.* **263**, 12638–12644 (1988).
- Byrd, T.F. & Horwitz, M.A. Regulation of transferrin receptor expression and ferritin content in human mononuclear phagocytes. Coordinate upregulation by iron transferrin and downregulation by interferon gamma. *J. Clin. Invest.* **91**, 969–976 (1993).
- Weiss, G., Wachter, H. & Fuchs, D. Linkage of cell-mediated immunity to iron metabolism. *Immunol. Today* **16**, 495–500 (1995).
- Vergne, A.F., Walz, A.J. & Miller, M.J. Iron chelators from mycobacteria (1954–1999) and potential therapeutic applications. *Nat. Prod. Rep.* **17**, 99–116 (2000).
- Olakanmi, O., Schlesinger, L.S., Ahmed, A. & Britigan, B.E. Intraphagosomal *Mycobacterium tuberculosis* acquires iron from both extracellular transferrin and intracellular iron pools. Impact of interferon-gamma and hemochromatosis. *J. Biol. Chem.* **277**, 49727–49734 (2002).
- Sun, H., Li, H.Y. & Sadler, P.J. Transferrin as a metal ion mediator. *Chem. Rev.* **99**, 2817–2842 (1999).
- Fadeev, E.A., Luo, M. & Groves, J.T. Synthesis, structure, and molecular dynamics of gallium complexes of schizokinen and the amphiphilic siderophore acinetoferrin. *J. Am. Chem. Soc.* **126**, 12065–12075 (2004).
- Murphy, D.J. The biogenesis and functions of lipid bodies in animals, plants and microorganisms. *Prog. Lipid Res.* **40**, 325–438 (2001).
- Dvorak, A.M. *et al.* Lipid bodies: cytoplasmic organelles important to arachidonate metabolism in macrophages and mast cells. *J. Immunol.* **131**, 2965–2976 (1983).
- De Voss, J.J. *et al.* The salicylate-derived mycobactin siderophores of *Mycobacterium tuberculosis* are essential for growth in macrophages. *Proc. Natl. Acad. Sci. USA* **97**, 1252–1257 (2000).
- Xu, G., Martinez, J.S., Groves, J.T. & Butler, A. Membrane affinity of the amphiphilic marinobactin siderophores. *J. Am. Chem. Soc.* **124**, 13408–13415 (2002).
- Luo, M., Fadeev, E.A. & Groves, J.T. Membrane dynamics of the amphiphilic siderophore, acinetoferrin. *J. Am. Chem. Soc.* **127**, 1726–1736 (2005).
- Moody, D.B. *et al.* T cell activation by lipopeptide antigens. *Science* **303**, 527–531 (2004).
- Testa, U. *et al.* Iron up-modulates the expression of transferrin receptors during monocyte-macrophage maturation. *J. Biol. Chem.* **264**, 13181–13187 (1989).
- Mulero, V. & Brock, J.H. Regulation of iron metabolism in murine J774 macrophages: role of nitric oxide-dependent and independent pathways following activation with gamma interferon and lipopolysaccharide. *Blood* **94**, 2383–2389 (1999).
- Crosa, J.H. & Walsh, C.T. Genetics and assembly line enzymology of siderophore biosynthesis in bacteria. *Microbiol. Mol. Biol. Rev.* **66**, 223–249 (2002).
- De Voss, J.J., Rutter, K., Schroeder, B.G. & Barry, C.E. Iron acquisition and metabolism by mycobacteria. *J. Bacteriol.* **181**, 4443–4451 (1999).
- Ratledge, C. Iron, mycobacteria and tuberculosis. *Tuberculosis (Edinb.)* **84**, 110–130 (2004).
- Olakanmi, O., Britigan, B.E. & Schlesinger, L.S. Gallium disrupts iron metabolism of mycobacteria residing within human macrophages. *Infect. Immun.* **68**, 5619–5627 (2000).